Acta Oceanol. Sin., 2018, Vol. 37, No. 1, P. 73–88
DOI: 10.1007/s13131-017-1118-8
http://www.hyxb.org.cn
E-mail: hyxbe@263.net

Geochemical and Sr-Nd-Pb isotopic compositions of volcanic rocks from the Iheya Ridge, the middle Okinawa Trough: implications for petrogenesis and a mantle source

LI Xiaohui[1, 2], ZENG Zhigang[1, 3]*, CHEN Shuai[1], MA Yao[1], YANG Huixin[1], ZHANG Yuxiang[1, 2], CHEN Zuxing[1, 2]

[1] Key Laboratory of Marine Geology and Environment, Institute of Oceanology, Chinese Academy of Sciences, Qingdao 266071, China

[2] University of Chinese Academy of Sciences, Beijing 100049, China

[3] Laboratory for Marine Mineral Resources, Qingdao National Laboratory for Marine Science and Technology, Qingdao 266071, China

Received 19 June 2017; accepted 31 August 2017

Abstract

As an active back-arc basin, the Okinawa Trough is located in the southeastern region of the East China Sea shelf and is strongly influenced by the subduction of the Philippine Sea Plate. Major element, trace element and Sr-Nd-Pb isotopic composition data are presented for volcanic rocks from the Iheya Ridge (IR), the middle Okinawa Trough. The IR rocks record large variations in major elements and range from basalts to rhyolites. Similar trace element distribution characteristics together with small variations in $^{87}Sr/^{86}Sr$ (0.703 862–0.704 884), $^{144}Nd/^{143}Nd$ (0.512 763–0.512 880) and Pb isotopic ratios, demonstrate that the IR rocks are derived from a similar magma source. The fractional crystallization of olivine, clinopyroxene, plagioclase, and amphibole, as well as accessory minerals, can reasonably explain the compositional variations of these IR rocks. The simulations suggest that approximately 60% and 75% fractionation of an evolved basaltic magma can produce trace element compositions similar to those of the intermediate rocks and acid rocks, respectively. The analysis of their Sr-Nd-Pb isotopic content ratios suggest that the source of the rocks from the IR is close to the depleted mantle (DM) but extends to the enriched mantle (EMII), indicating that the mantle source of these rocks is a mixture between the DM and EMII end members. The simulations show that the source of the IR volcanic rocks can be best interpreted as the result of the mixing of approximately 0.8%–2.0% subduction sediment components and 98.0%–99.2% mantle-derived melts.

Key words: basic to intermediate-acid rocks, fractional crystallization, subduction sediment components, Iheya Ridge, Okinawa Trough

Citation: Li Xiaohui, Zeng Zhigang, Chen Shuai, Ma Yao, Yang Huixin, Zhang Yuxiang, Chen Zuxing. 2018. Geochemical and Sr-Nd-Pb isotopic compositions of volcanic rocks from the Iheya Ridge, the middle Okinawa Trough: implications for petrogenesis and a mantle source. Acta Oceanologica Sinica, 37(1): 73–88, doi: 10.1007/s13131-017-1118-8

1 Introduction

Most volcanic rocks generated from subduction settings record complex magma source compositions, which are typically affected by subduction components, including altered oceanic crust, pelagic sediments, slab-derived fluids and/or melts (Plank, 2005), and even continental crust materials. Studies of the types of mantle sources, magma evolution and the injection of subduction components, as well as the interactions between the mantle and the crust, have become important in understanding the tectonic evolution of back-arc basins (Shinjo and Kato, 2000; Plank, 2005; Yan and Shi, 2014).

The Okinawa Trough (OT), which is influenced by the extension of the Asian continental lithosphere, is a spreading back-arc basin of the Ryukyu trench-arc-basin system (Shinjo, 1999). Since the 1970s, many investigations of the OT have been performed (Lee et al., 1980; Letouzey and Kimura, 1985), which have yielded abundant geophysical and geological data. However, compared with studies of its hydrothermal region, its tectonic

Foundation item: The National Basic Research Program (973 Program) of China under contract No. 2013CB429700; the National Natural Science Foundation of China under contract Nos 41325021 and 41706052; the National Program on Global Change and Air-Sea Interaction under contract No. GASI-GEOGE-02; the Strategic Priority Research Program of the Chinese Academy of Sciences under contract No. XDA11030302; the Special Fund for the Taishan Scholar Program of Shandong Province under contract No. ts201511061; the AoShan Talents Program supported by Qingdao National Laboratory for Marine Science and Technology under contract No. 2015ASTP-0S17; the Innovative Talent Promotion Program under contract No. 2012RA2191; the Science and Technology Development Program of Shandong Province under contract No. 2013GRC31502; the Scientific and Technological Innovation Project Financially supported by Qingdao National Laboratory for Marine Science and Technology under contract Nos 2015ASKJ03 and 2016ASKJ13; the National High Level Talent Special Support Program, the CAS/SAFEA International Partnership Program for Creative Research Teams, and Qingdao Collaborative Innovation Center of Marine Science and Technology.
*Corresponding author, E-mail: zgzeng@ms.qdio.ac.cn

and petrologic activities have received less attention (Yan and Shi, 2014), which has resulted in many controversies about the types of mantle sources and evolution of magma within this region (Ishizuka et al., 1990; Shinjo, 1999; Huang et al., 2006; Zeng et al., 2010). As a probe of deep mantle activity, volcanic rocks provide direct evidence of the tectonic activity and geodynamic mechanisms in the OT (Yan and Shi, 2014; Yang and Fang, 2015). Shinjo (1999) analyzed the Sr-Nd isotopic compositions of basalt and suggested that E-MORB and melts derived from the subducted slab are the primary magma sources in the middle OT. Huang et al. (2006) researched the Sr-Nd isotopic compositions of volcanic rocks in the northern and middle OT and determined that magmatic material in the OT is derived from a PREMA mantle source. An intermediate composition between arc magma and N-MORB also may be the source of magma within the OT (Ishizuka et al., 1990). Zeng et al. (2010) considered that the basalt derived from the northern OT was produced by the interaction between Indian Ocean-type mantle and the enrichment of the continental lithosphere. In addition, Yan and Shi (2014) summarized different types of volcanic rocks and proposed that the magma source of the southern OT is Indian Ocean-type mantle that has been reformed by EMII; moreover, Indian Ocean-type mantle, EMI, and EMII comprise the sources of the middle OT, while the sources of the northern OT consist of the PREMA mantle and EMII. In addition, the processes of magma evolution in the OT, such as fractional crystallization, magma mixing and assimilation and fractional crystallization (AFC), have attracted the attention of many scholars (Li et al., 1997; Zhai et al., 1997).

In this paper, based on the observations of thin sections and the analyses of major elements, trace elements and Sr-Nd-Pb isotopes, we have carried out a petrographic and geochemical study of the IR volcanic rocks collected from the middle OT. We believe that these results can be used to gain insight into the magma evolution process and to provide evidence with which to determine the magma sources of the IR rocks.

2 Geologic setting and samples

2.1 *Geologic setting*

The OT is located at the southern tip of the East China Sea shelf, where the Philippine Sea Plate is subducting beneath the Eurasian Plate, with an output scope that is approximately 1 200 km long and 100–150 km wide (Fig. 1) (Shinjo, 1999; Li, 2001). It is a nascent back-arc basin that yields ages that are generally younger than 1 Ma, according to the geochronologic analysis of its volcanic rocks (Ishikawa et al., 1991; Shinjo, 1999). The area features many normal faults, as well as crustal thinning and rifting (Okino et al., 2002). Along the axis of the OT, several en-echelon extensional grabens have been identified (Shinjo and Kato, 2000). Geophysical data record the following geological characteristics: thin crustal thickness, negative geomagnetic anomalies, gravity anomalies and abnormally high heat flow values (Yamano et al., 1989; Li, 2001). The characteristics of these anomalies may reflect the uplifting of the upper mantle and the depression of the basement (Yan and Shi, 2014).

The OT is divided into three parts, based on its tectonic characteristics; from the southwest to the northeast, these are the northern Okinawa Trough (NOT), the middle Okinawa Trough (MOT) and the southern Okinawa Trough (SOT). The boundary between the NOT and the MOT is the Tokara Strait, and the boundary between the MOT and the SOT is the Kerama Gap (Shinjo, 1999; Li, 2001). Additionally, the NOT corresponds to a crustal stretching phase, the MOT is related to the propagating

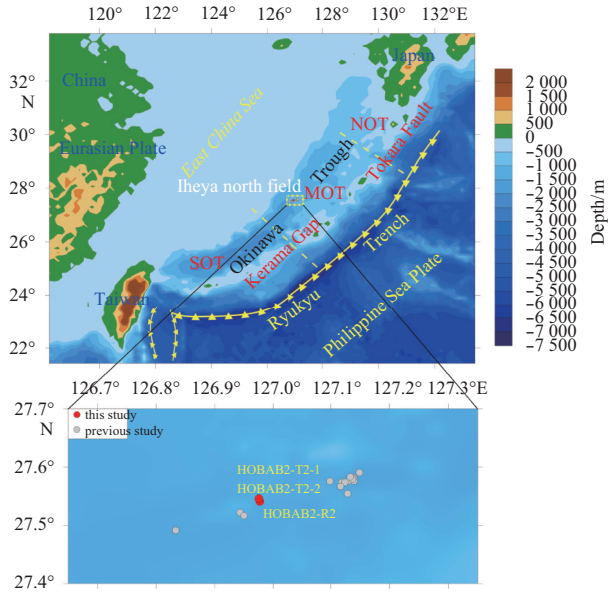

Fig. 1. Regional bathymetric map of the Ryukyu trench-arc-basin system, which shows the location, tectonic setting, and depth of the OT (after Shinjo, 1999). A detailed bathymetric depth map of the IR is displayed on a larger scale. The sampling locations used in this study and previous studies are also shown.

rift phase, and the SOT records the characteristics of the initial spreading phase and may have been influenced by the arc-continent collision at the Taiwan Island (Miki et al., 1990; Wang et al., 1999; Yan and Shi, 2014). The crustal thickness differs between these three regions and gradually increases from the SOT (≈18 km) to the NOT (≈30 km) (Wang et al., 1998).

The evolutionary stages of extension within the OT have been divided into three parts: (1) the middle to late Miocene (6.0–7.0 Ma), which is the major tectonic phase of the extension that mainly occurs in the MOT and NOT and may be connected with the opening of the Sea of Japan (Shinjo, 1999); (2) the early Pleistocene (2.0–0.1 Ma), which mainly produces the extensional fractures of the SOT; and (3) the late Pleistocene to the Holocene (0.1–0 Ma), which formes the embedded nature of the SOT and the normal faults that cut the shallow strata (Kimura, 1985; Letouzey and Kimura, 1986; Sibuet et al., 1987).

The OT produced strong magmatic activity and has generated many volcanic rocks (Gao et al., 2009). These volcanic rocks mainly record bimodal characteristics, comprising a basaltic-rhyolitic suite in the MOT (Li et al., 1997). The types of the rocks that have been produced here include basalt, dacite, rhyolite and a small amount of andesite (Huang et al., 2006).

The IR (27°32.5′N, 126°58.5′E) lies approximately 120 km to the NNW of the Okinawa Island (Fig. 1). Many small conical knolls and small elongated volcanic ridges have been identified in the IR, which may imply the presence of substantial volcanic activity in this region (Fig. 1).

2.2 *Samples and petrography*

The three samples studied in this paper were collected from the IR using a TV-grab sampler during the R/V *Kexue* cruise in 2014. At the same time, we gathered 16 volcanic rocks that represent samples with Sr-Nd isotopic compositions that were previously published in this region (Table 1).

The hand specimen (Fig. 2) of the basalt sample (HOBAB2-

Table 1. Sampling locations of the IR rocks from the MOT

Sample	North latitude	East longitude	Depth/m	Reference
HOBAB2-R2	27°32′28.21″	126°58′37.28″	1 309.7	this study
HOBAB2-T2-1	27°32′45.63″	126°58′31.07″	1 238	this study
HOBAB2-T2-1	27°32′45.63″	126°58′31.07″	1 238	this study
CB6-23	27°34′24.60″	127°07′7.20″	1 450	Ishizuka et al. (1990)
CB6-22	27°34′36.60″	127°07′54.00″	1 450	Ishizuka et al. (1990)
A2B	27°34′25.20″	127°07′27.00″	1 336	Kimura et al. (1987)
A6	27°31′19.80″	126°56′35.99″	967	Kimura et al. (1987)
12-1YK	27°34′55.80″	127°08′18.60″	1 630	Kimura et al. (1986)
12-2YK	27°34′52.20″	127°08′10.20″	1 535	Kimura et al. (1986)
CB6-20	27°34′34.20″	127°08′22.20″	1 600	Ishizuka et al. (1990)
CB6-25	27°33′16.20″	127°07′43.80″	1 450	Ishizuka et al. (1990)
13-3YK	27°34′46.20″	127°08′13.80″	1 538	Kimura et al. (1986)
CB6-24	27°34′21.00″	127°05′55.20″	1 300	Ishizuka et al. (1990)
287-2A	27°29′30.00″	126°49′59.99″	1 380	Kimura et al. (1991)
287-2C	27°29′30.00″	126°49′59.99″	1 380	Kimura et al. (1991)
A-6	27°31′19.80″	126°56′35.99″	967	Kimura et al. (1987)
A-2-a	27°34′00.00″	127°07′1.20″	–	Honma et al. (1991)
A-1-b	27°34′00.00″	127°07′1.20″	–	Honma et al. (1991)
12-3	27°35′00.00″	127°07′59.99″	–	Honma et al. (1991)

Note: –means not collected.

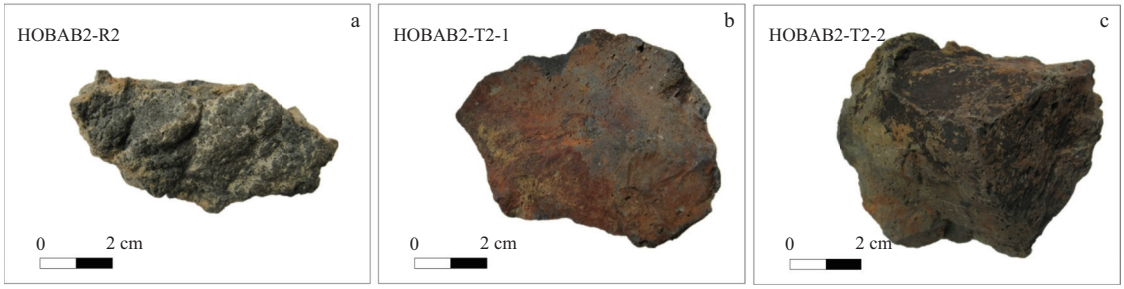

Fig. 2. Pictures of hand specimens of IR rocks analyzed in this study.

R2) has a massive structure and is approximately 8 cm×4 cm×3 cm in size. The color of the surface of the rock is taupe; although it is covered in sediment, the color of its fresh face is grayish-black and it is strongly vesicular (Fig. 2a). Small vesicles are evenly distributed throughout the sample. The andesite sample (HOBAB2-T2-1) is massive and is less vesicular than the basalt. It is approximately 9 cm×9 cm×6 cm in size; its surface is red-brown in color and its fresh face is gray (Fig. 2b). The other andesite sample (HOBAB2-T2-2) has similar characteristics as HOBAB2-T2-1; it is approximately 9 cm×7 cm×7 cm in size and is yellowish-brown on the surface but gray on its fresh face (Fig. 2c).

All of the samples were sectioned and observed under a polarizing microscope. Under the microscope, the basalt sample (HOBAB2-R2) (Figs 3a and b) is characterized by its porphyritic texture; its main phenocrystic minerals are olivine (Ol, ≈5%), clinopyroxene (Cpx, ≈1%), and plagioclase (Pl, ≈5%). Olivine is characterized by the presence of significant cracks. The matrix minerals mainly comprise plagioclase, ilmenite, apatite, and magnetite. The phenocrysts range in size from 50 to 500 μm and show euhedral to subhedral textures. The two andesite samples (HOBAB2-T2-1, HOBAB2-T2-2) (Figs 3c, d, e and f) have similar characteristics; both record porphyritic textures and matrixes that mainly comprise microcrystalline plagioclase. Their phenocrysts mainly comprise Ol (≈1%), Cpx (≈5%) and Pl (≈10%). Clinopyroxene is subhedral and ranges in size from 100 to 400 μm, while plagioclase is euhedral to subhedral and ranges in size from 10 to 1 000 μm.

3 Analytical methods

First, we cleaned each fresh sample, cut it into thin slices, placed it in an ultrasonic cleaning machine and cleaned it for approximately 15 min to remove any sediment in the pores. Then, the sample was immersed in anhydrous ethanol to remove organic matter; after this, the sample was removed and dried. Next, the slices were placed in dilute hydrochloric acid and heated in a water bath to ca. 60°C, where they were kept for 1–2 h to eliminate secondary carbonates. Finally, the slices were broken into rock chips, which soaked in hot water for 7–10 d; the water was constantly changed until no precipitate was generated after the addition of $AgNO_3$ (Huang et al., 2006). The rock chips were pulverized into powders with a size of 200 mesh using an agate mill, which were then prepared for analyses of their major element, trace element and Sr-Nd-Pb isotopic compositions.

3.1 *Major and trace elements*

The major element compositions of whole-rock samples were tested using a standard X-ray fluorescence (XRF) procedure at the Test and Analysis Center of Jilin University, Changchun, China. First, approximately 0.5 g of each sample powder and approximately 5 g of $Li_2B_4O_7$ were mixed to manufacture specially

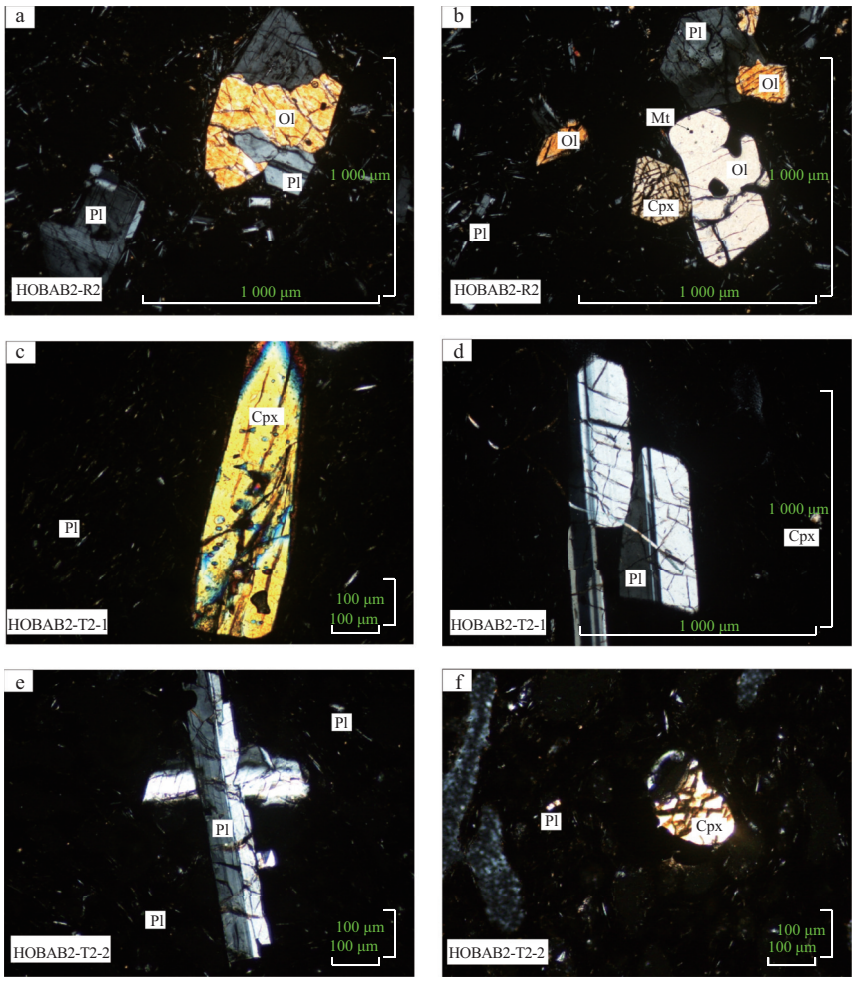

Fig. 3. Photomicrographs of the IR rocks analyzed in this study. Representative photomicrographs of HOBAB2-R2 (a, b), representative photomicrographs of HOBAB2-T2-1 (c, d) and representative photomicrographs of HOBAB2-T2-2 (e, f). Ol indicates olivine, Mt magnetite, Cpx clinopyroxene, and Pl plagioclase.

made glass disks. Then, the disk was analyzed and the major elements were determined using an AXIOS minerals spectrometer, which yielded analytical uncertainties ranging from 1% to 3%. Whole-rock trace element concentrations were measured using the inductively coupled-plasma mass spectrometer (ICP-MS) at the Institute of Oceanology, Chinese Academy of Sciences, Qingdao. Approximately 50 mg of each rock powder was dissolved in a mixture of concentrated HNO_3 and HF in a teflon vessel and maintained at about 150°C for 5 d. International standards used for whole-rock analyses are the Columbia River basalt (BCR-2) and basalts from the Hawaiian Volcanic Observatory (BHVO-2). The detection limits for rare earth elements (REE) and other trace elements were 10^{-12}–10^{-9}; the analytical precision of REE analyses was less than 2.6% and those of other trace elements were less than 3%.

3.2 *Sr-Nd-Pb isotopes*

Sr-Nd-Pb isotopic compositions were analyzed at Key Laboratory of the Chinese Academy of Sciences (CAS) for Crust-Mantle Materials and Environments in the University of Science and Technology of China, Anhui. The measurements of Rb-Sr, Sm-Nd and Pb isotopes were performed using a Finnigan MAT262 thermal ionization mass spectrometer (TIMS). The standard values of $^{86}Sr/^{88}Sr$=0.119 4 and $^{146}Nd/^{144}Nd$=0.721 9 were used to correct the measured $^{87}Sr/^{86}Sr$ and $^{143}Nd/^{144}Nd$ ratios. Repeated measurements of the NBS987 and La Jolla standards were used to correct the mass fractionation of Sr and Nd. The analytical precision of the ratios of $^{87}Rb/^{86}Sr$ and $^{147}Sm/^{144}Nd$ was better than 0.5% and 0.003%, respectively. The conventional AG50 1×8 anion exchange technology was used to separate Pb isotopes. The NBS981 Pb standards yielded $^{206}Pb/^{204}Pb$, $^{207}Pb/^{204}Pb$ and $^{208}Pb/^{204}Pb$ values of 16.932±1 (2σ), 15.485±1 (2σ) and 36.685±1 (2σ), respectively. The analytical precision of the Pb isotopic ratios was better than 0.01%, and blank levels of total Pb isotopes were less than 0.1 ng.

4 Results

4.1 *Major and trace elements*

The major and trace element concentrations of the rocks collected from the IR are listed in Table 2, in which data cited from previous studies in this region are also listed. On a total alkali versus silica classification diagram (Fig. 4a), the IR rocks record large compositional variations and range from basic rocks (basalt) to acid rocks (rhyolite); they also plot as a subalkaline series (SiO_2=49.20–75.04 wt%; Na_2O+K_2O=2.53–7.26 wt%). On K_2O versus SiO_2 diagrams (Fig. 4b), the IR rocks range from the low-potassium arc-tholeiitic series to the medium-potassium

calc-alkaline series. The basic rocks straddle the boundary of the low-potassium arc-tholeiitic series and the medium-potassium calc-alkaline series, and the intermediate-acid rocks fall within the medium-potassium calc-alkaline series. Basic rocks are characterized by high concentrations of CaO (9.93–12.21 wt%), MgO (5.66–8.62 wt%), and FeO_t (8.34–10.56 wt%), which yield $Mg^{\#}$ [$Mg^{\#}$=Mg/(Mg+Fe)] values ranging from 0.52–0.62; they also record low concentrations of SiO_2 (49.20–52.38 wt%), K_2O (0.42–0.54 wt%), and N_2O (2.11–3.18 wt%). Intermediate rocks have relatively high concentrations of SiO_2 (56.90–61.63 wt%) and K_2O (1.02–1.87 wt%), but relatively low concentrations of MgO (2.06–4.36 wt%) and FeO_t (6.13–9.99 wt%), which yield $Mg^{\#}$ values ranging from 0.38–0.48. Acid rocks record the highest concentrations of SiO_2 (67.72–75.04 wt%) and K_2O (2.23–2.88 wt%), but the lowest concentrations of CaO (1.86–3.04 wt%), FeO_t (2.20–3.90 wt%), MgO (0.40–0.92 wt%), and TiO_2 (0.27–0.54 wt%),

Table 2. Major and trace element compositions of the IN rocks from the MOT

Sample	This study			Shinjo et al. (1999)				Shinjo and Kato (2000)		
	HOBAB2-R2	HOBAB2-T2-1	HOBAB2-T2-2	CB6-22	CB6-23	A2B	A6	21-1YK	12-2YK	CB6-20
SiO_2	52.38	61.63	61.01	49.20	51.08	50.93	51.92	70.16	72.11	75.04
Al_2O_3	17.26	15.61	15.48	16.82	16.05	16.26	16.96	13.73	14.44	13.90
FeO_t	8.34	6.13	6.37	9.69	10.12	10.05	10.56	2.58	2.68	2.2
CaO	9.93	5.05	5.08	11.33	11.84	11.72	10.18	2.12	2.20	1.86
MgO	5.66	2.06	2.21	7.68	8.62	8.38	6.32	0.62	0.51	0.40
K_2O	0.54	1.87	1.78	0.42	0.42	0.42	0.44	2.65	2.67	2.88
Na_2O	2.89	4.51	4.47	2.15	2.11	2.13	2.65	4.61	4.15	4.29
TiO_2	1.14	1.07	1.10	0.96	0.99	1.01	1.16	0.35	0.35	0.27
P_2O_5	0.22	0.26	0.25	0.16	0.17	0.17	0.24	0.06	0.07	0.07
MnO	0.17	0.14	0.14	0.16	0.17	0.17	0.18	0.13	0.07	0.06
LOI	1.05	1.37	1.54	0.56	0.62	0.47	1.43	2.73	2.18	2.72
SUM	99.74	99.85	99.56	98.58	101.57	101.24	100.61	97.01	99.25	100.94
$Mg^{\#}$	0.55	0.38	0.38	0.59	0.61	0.60	0.52	0.30	0.26	0.25
Sc	29.6	15.9	15.7	38.0	37.4	38.9	35.3	5.10	4.80	3.70
V	259	133	156	289	266	285	254	28.0	20.0	12.0
Cr	152	10.3	2.32	246	295	276	137	68.0	3.00	2.00
Co	31.7	12.5	13.5	41.0	43.0	41.0	34.0	5.00	3.00	2.00
Ni	46.8	5.24	3.95	83.0	104	93.0	50.0	43.0	2.00	1.00
Cu	61.3	26.0	28.0	–	–	–	–	–	–	–
Zn	100	90.6	93.1	–	–	–	–	–	–	–
Rb	10.6	38.6	31.8	8.80	8.60	7.90	8.30	83.8	82.1	89.9
Sr	263	193	196	249	241	240	242	125	125	105
Y	22.6	36.4	35.4	21.1	20.3	20.2	27.1	23.8	23.5	22.6
Zr	81.9	198	203	58.0	55.0	56.0	93.0	244	177	167
Nb	3.38	7.53	7.68	3.50	3.30	3.40	4.10	6.50	6.60	6.50
Cs	0.530	1.84	1.76	0.280	0.270	0.280	0.410	3.09	3.10	3.24
Ba	89.4	252	243	75.0	71.0	72.0	95.0	421	396	419
La	7.17	16.8	15.5	5.51	5.21	5.34	8.55	17.3	16.2	16.6
Ce	17.6	37.5	36.1	13.2	12.5	12.7	20.6	35.0	32.5	32.4
Pr	2.49	4.92	4.66	1.92	1.82	1.84	2.88	3.87	3.75	3.64
Nd	11.7	21.5	20.3	9.20	8.73	8.77	13.3	14.4	14.2	13.6
Sm	3.16	5.27	5.09	2.66	2.56	2.58	3.56	3.07	3.08	2.90
Eu	1.17	1.49	1.52	1.03	0.990	0.990	1.25	0.780	0.810	0.720
Gd	3.19	5.23	5.09	3.10	2.96	2.99	3.98	3.06	3.09	2.89
Tb	0.660	0.980	0.990	0.540	0.520	0.520	0.680	0.520	0.530	0.490
Dy	3.74	5.92	5.76	3.44	3.29	3.28	4.28	3.28	3.33	3.14
Ho	0.860	1.37	1.33	0.730	0.700	0.700	0.920	0.720	0.730	0.690
Er	2.28	3.73	3.65	2.11	2.03	2.05	2.69	2.27	2.26	2.16
Tm	0.360	0.610	0.600	0.320	0.310	0.300	0.410	0.380	0.380	0.360
Yb	2.22	3.86	3.67	1.97	1.90	1.90	2.56	2.62	2.51	2.41
Lu	0.340	0.590	0.570	0.310	0.290	0.290	0.400	0.420	0.410	0.390
Hf	2.02	4.95	4.70	1.48	1.42	1.40	2.15	5.13	4.29	4.13
Ta	0.170	0.440	0.430	0.230	0.230	0.230	0.250	0.580	0.600	0.610
Pb	2.11	5.57	4.85	1.51	1.42	1.54	2.32	9.10	6.68	6.83
Th	0.840	4.74	4.39	0.670	0.640	0.580	0.770	7.51	7.08	7.62
U	0.290	1.22	1.14	0.210	0.200	0.180	0.200	1.86	1.72	1.83

to be continued

Continued from Table 2

Sample	Shinjo and Kato (2000)					Honma et al. (1991)			
	CB6-25	13-3YK	CB6-24	287-2A	287-2C	A-6	A-2-a	A-1-b	12-3
SiO_2	72.38	67.72	59.61	58.56	56.90	51.90	49.68	49.74	72.37
Al_2O_3	14.32	15.41	15.87	16.10	16.09	16.67	15.93	16.11	13.94
FeO_t	3.10	3.90	8.42	9.72	9.99	9.50	9.02	8.63	2.33
CaO	2.33	3.04	6.97	7.05	6.91	10.46	12.21	11.91	2.10
MgO	0.59	0.92	4.36	3.41	3.35	5.84	7.32	7.72	0.53
K_2O	2.60	2.23	1.24	1.10	1.02	0.42	0.42	0.44	2.51
Na_2O	4.11	4.29	3.40	3.91	3.85	3.18	2.60	2.31	4.31
TiO_2	0.36	0.54	0.87	1.29	1.30	1.16	0.99	0.97	0.37
P_2O_5	0.07	0.14	0.21	0.38	0.37	0.19	0.22	0.15	0.14
MnO	0.07	0.10	0.15	0.19	0.19	0.20	0.18	0.17	0.06
LOI	1.55	1.87	0.88	1.08	0.95	–	–	–	–
SUM	99.93	98.29	101.10	101.71	99.97	100.86	99.90	99.43	100.00
$Mg^{\#}$	0.26	0.30	0.48	0.39	0.38	0.53	0.59	0.62	0.29
Sc	5.20	7.50	21.6	24.0	24.5	–	–	–	–
V	30.0	41.0	164	172	175	294	320	226	15.4
Cr	5.00	5.00	111	27.0	32.0	171	288	275	6.70
Co	5.00	6.00	23.0	19.0	19.0	–	–	–	–
Ni	2.00	2.00	45.0	10.0	11.0	59.7	79.3	92.1	–
Cu	–	–	–	–	–	59.4	78.6	–	2.80
Zn	–	–	–	–	–	96.5	84.1	–	38.9
Rb	79.9	67.6	34.5	26.7	26.0	12.0	12.4	12.0	80.9
Sr	125	166	226	291	285	293	292	289	135
Y	23.5	28.1	27.9	38.9	38.6	31.4	23.0	23.0	22.2
Zr	233	194	149	148	146	121	71.1	67.6	201
Nb	6.10	7.00	5.10	6.70	6.60	–	–	–	–
Cs	2.91	2.48	1.30	1.09	1.10	–	–	–	–
Ba	393	352	206	197	193	–	–	–	–
La	16.6	16.4	11.7	15.2	15.0	–	–	–	–
Ce	33.0	34.5	26.1	35.1	34.6	–	–	–	–
Pr	3.75	4.08	3.39	4.74	4.69	–	–	–	–
Nd	14.1	16.2	14.7	21.2	20.9	13.9	9.50	9.00	13.9
Sm	3.04	3.71	3.71	5.37	5.31	3.70	2.70	2.60	3.00
Eu	0.780	1.05	1.21	1.77	1.75	–	–	–	–
Gd	3.03	3.78	3.95	5.82	5.80	–	–	–	–
Tb	0.520	0.640	0.680	0.980	0.970	–	–	–	–
Dy	3.30	4.02	4.30	6.08	6.03	–	–	–	–
Ho	0.730	0.870	0.930	1.31	1.29	–	–	–	–
Er	2.29	2.68	2.78	3.80	3.77	–	–	–	–
Tm	0.380	0.430	0.430	0.590	0.580	–	–	–	–
Yb	2.61	2.87	2.81	3.68	3.67	–	–	–	–
Lu	0.430	0.460	0.450	0.570	0.570	–	–	–	–
Hf	5.13	4.44	3.41	3.56	3.47	–	–	–	–
Ta	0.540	0.560	0.370	0.440	0.420	–	–	–	–
Pb	6.96	5.97	3.93	3.54	3.39	–	–	–	–
Th	7.20	5.87	3.10	2.77	2.59	–	–	–	–
U	1.82	1.44	0.810	0.720	0.640	–	–	–	–

Note: Major element concentration is in wt%, trace element concentration in 10^{-6}. FeO_t represents total FeO given in Fe^{2+} and – not collected.

which yield $Mg^{\#}$ values ranging from 0.25–0.30.

The primitive mantle-normalized spider diagrams record the enrichment of LILE compared with HFSE and REE and exhibit peaks at Rb, Pb, and K (Fig. 5). These enrichments are coupled with relative depletions of Nb, Ta, and Ti. On spider diagrams, the three lithologies of these rocks record nearly parallel trace element distribution patterns for all elements except for P, Ti, Zr, Hf, Eu, and Sr (Fig. 5). Compared with the basic rocks, the intermediate and acid rocks record positive Zr, Hf, and Eu anomalies but depletions of P, Ti, and Sr. The ∑REE concentration is 43.85×10^{-6}–66.00×10^{-6} in basic rocks, 75.87×10^{-6}–109.77×10^{-6} in intermediate rocks and 82.04×10^{-6}–91.65×10^{-6} in acid rocks. The REE profiles yield $(La/Yb)_N$ ratios of 1.96–2.39 for basic rocks, 2.93 to 3.12 for intermediate rocks and 4.09–4.83 for acid rocks, which indicates that the fractionation between LREE and HREE is higher in acid rocks than it is in basic rocks (Figs 5b, d and f). Fur-

thermore, the REE patterns of basic rocks (Figs 5b, d and f) reveal slightly positive Eu anomalies [δEu=1.01–1.11, δEu=2Eu$_N$/(Sm$_N$+Gd$_N$)], while those of intermediate and acid rocks record negative Eu anomalies, in which δEu=0.86–0.96 and 0.75–0.85, re-

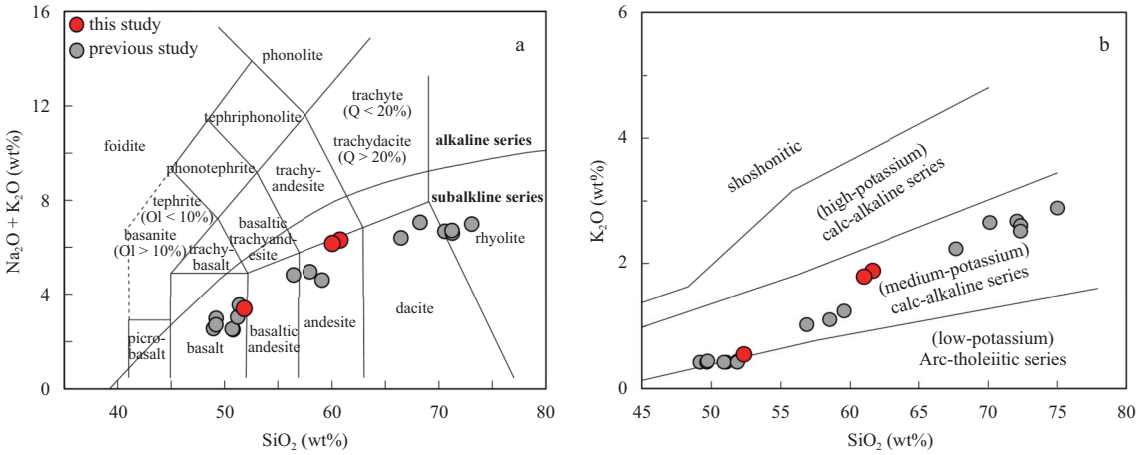

Fig. 4. Petrological diagrams of the IR volcanic rocks. a. Plots of IR rocks on the total alkalis versus silica classification diagram [(Na_2O+K_2O) vs SiO_2)] of Le Maitre (1989). The boundary between alkaline and subalkaline rocks is from Irvine and Baragar (1971). The diagram shows that the IR volcanic rocks belong to the subalkaline series and record large compositional differences between basalt and rhyolite. b. K_2O (wt%) versus SiO_2 (wt%) diagram for IR volcanic rocks. The diagram shows that the IR volcanic rocks range from the low-K arc-tholeiitic series to the medium-K calc-alkaline series.

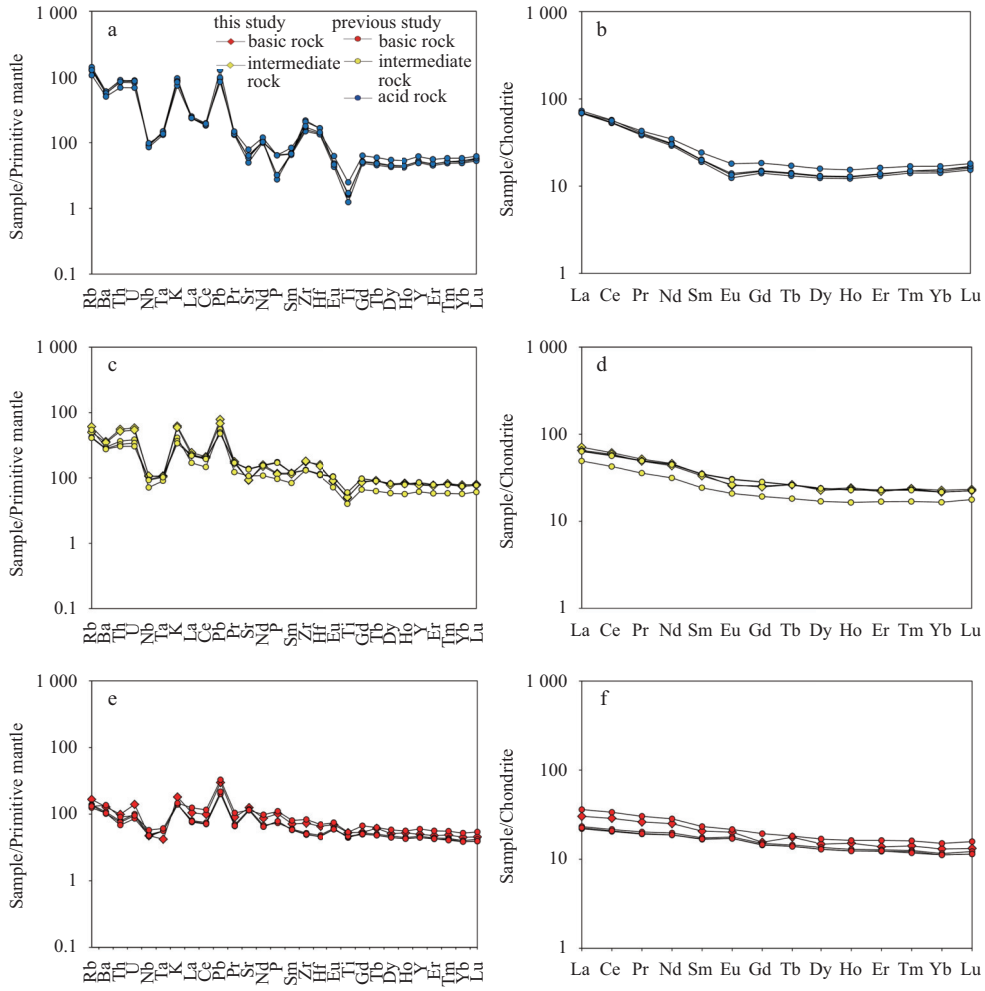

Fig. 5. Trace element patterns (a, c and e) normalized to primitive mantle concentrations and REE patterns (b, d and f) normalized to chondritic values for the IR rocks. Primitive mantle and chondritic values are from Sun and McDonough (1989).

Table 3. Sr-Nd-Pb isotopic compositions of the IN rocks from the MOT

Sample	$^{87}Sr/^{86}Sr$ (2σ)	$^{143}Nd/^{144}Nd$ (2σ)	εNd(0)	$^{206}Pb/^{204}Pb$ (2σ)	$^{207}Pb/^{204}Pb$ (2σ)	$^{208}Pb/^{204}Pb$ (2σ)
This study						
HOBAB2-R2	0.704 188±14	0.512 763±09	2.44	18.493 2±16	15.680 2±18	38.814 0±57
HOBAB2-T2-1	0.704 522±14	0.512 865±13	4.43	18.505 5±12	15.648 1±12	38.730 9±34
HOBAB2-T2-2	0.704 628±14	0.512 811±09	3.37	18.523 6±14	15.654 8±15	38.767 6±42
Shinjo et al. (1999)						
CB6-22	0.703 892	0.512 870	4.53	–	–	–
CB6-23	0.703 862	–	–	–	–	–
A2B	0.703 950	0.512 831	3.76	–	–	–
A6	0.704 044	0.512 827	3.69	–	–	–
Shinjo and Kato (2000)						
21-1YK	0.704 292	0.512 837	3.88	–	–	–
12-2YK	0.704 017	0.512 863	4.39	–	–	–
CB6-20	0.704 049	0.512 856	4.25	–	–	–
CB6-25	0.704 077	0.512 819	3.53	–	–	–
13-3YK	0.704 056	0.512 856	4.25	–	–	–
CB6-24	0.704 042	0.512 829	3.73	–	–	–
287-2A	0.704 252	0.512 806	3.28	–	–	–
287-2C	0.704 270	–	–	–	–	–
Honma et al. (1991)						
A-6	0.704 44±3	0.512 84±3	3.94	–	–	–
A-2-a	0.704 40±3	0.512 86±3	4.33	–	–	–
A-1-b	0.704 41±2	0.512 88±2	4.72	–	–	–
12-3	0.704 34±3	0.512 86±3	4.33	–	–	–

Note: –means not collected.

spectively.

4.2 *Sr-Nd-Pb isotopes*

Table 3 lists all of the whole-rock Sr-Nd-Pb isotopic compositions, as well as the previously published Sr-Nd isotopic ratios in IR rocks. All of the IR rocks record a small range of variation in Sr-Nd isotopic ratios; $^{87}Sr/^{86}Sr$ values range from 0.703 862 to 0.704 884, and $^{144}Nd/^{143}Nd$ values range from 0.512 763 (εNd: +2.44) to 0.512 88 (εNd: +4.72) (Table 3, Fig. 6a).

This paper presents the first Pb isotopic ratios measured in the volcanic rocks of the IR. In the basalt, the $^{206}Pb/^{204}Pb$ ratio is 18.493 2, that of $^{207}Pb/^{204}Pb$ is 15.680 2 and that of $^{208}Pb/^{204}Pb$ is 38.814 0. The two andesite samples have $^{206}Pb/^{204}Pb$ ratios of 18.505 5 and 18.523 6, $^{207}Pb/^{204}Pb$ ratios of 15.648 1 and 15.654 8, and $^{208}Pb/^{204}Pb$ ratios of 38.730 9 and 37.767 6 (Table 3, Figs 6c and d).

5 Discussion

5.1 *Source types of the IR rocks*

Isotopic ratios can be used to trace magma sources, as they do not change substantially during the evolution of the magmatic system (Shinjo et al., 2000). Figure 6a shows that rocks from the IR plot on the line extending from the DM to EMII; on the $^{207}Pb/^{204}Pb$-$^{206}Pb/^{204}Pb$ diagram (Fig. 6c) as well as on $^{208}Pb/^{204}Pb$-$^{206}Pb/^{204}Pb$ diagram (Fig. 6d), basic and intermediate rocks record a trend in which they point to EMII, which indicates that the mantle source of the IR rocks may represent a mixture between DM and fertile mantle end members (Shinjo et al., 2000). Meanwhile, Hoang and Uto (2006) proposed that the DM end member in the MOT may be Indian Ocean-type mantle, which is represented by Philippine Sea Plate basalt (Savov et al., 2006; Hickey-Vargas, 1991, 1995). Furthermore, the higher concentrations of Pb, Rb, and U and the relative depletions of Nb, Ta, and Ti recorded in these IR rocks may have been reformed by sedimentary components due to subduction zone magmatism, which can produce melts that are markedly relatively depleted in Nb, Ta, and Ti (Hu et al., 2016). Previous studies have also argued that the OT has definitely been strongly affected by subducted components (Yan and Shi, 2014).

In Figs 6a and b, we choose two end members, namely, a Philippine Sea MORB-type source (PSP) to represent the Indian MORB and pelagic sediment (PS) to represent the subduction sediment components (Ishizuka et al., 2007). Several geochemical methods have been developed in recent studies (Miller et al., 1994; Class et al., 2000; Pearce and Peate, 1995) that can be used to quantitatively assess the contributions of these two end members to the IR rocks. This detailed simulation process is shown in Fig. 6a. These calculations illustrate that the contribution of the subduction sediment components is approximately 0.8%–2.0%, while 98.0%–99.2% mantle-derived melts were incorporated into the IR rock source. This result can also be seen on the $^{87}Sr/^{86}Sr$-$^{206}Pb/^{204}Pb$ diagram (Fig. 6b), as the isotopic ratios of the basaltic and andesitic rocks plot on the simulated evolution line, which is limited by the different end members of the PSP and the PS.

5.2 *Subduction sediment components*

Before discussing the evolution of the magma, it is necessary to determine whether these rocks have been affected by crustal contamination. The characteristics of the enrichment of the LILE, Pb and Sr but depletion of Nb, Ta, and Ti (Fig. 5) in the IR rocks are close to the distribution pattern of trace elements in the continental crust (Rudnick and Gao, 2003). Many studies have shown that if significant contamination or magma mixing processes exist between mantle melts and continental crust materials, then the $^{87}Sr/^{86}Sr$ ratios of volcanic rocks will vary with SiO_2, while their $^{143}Nd/^{144}Nd$ ratios will vary inversely with SiO_2 (Guo et al., 2014, 2016; Hu et al., 2016; Yang et al., 2017). However, as is

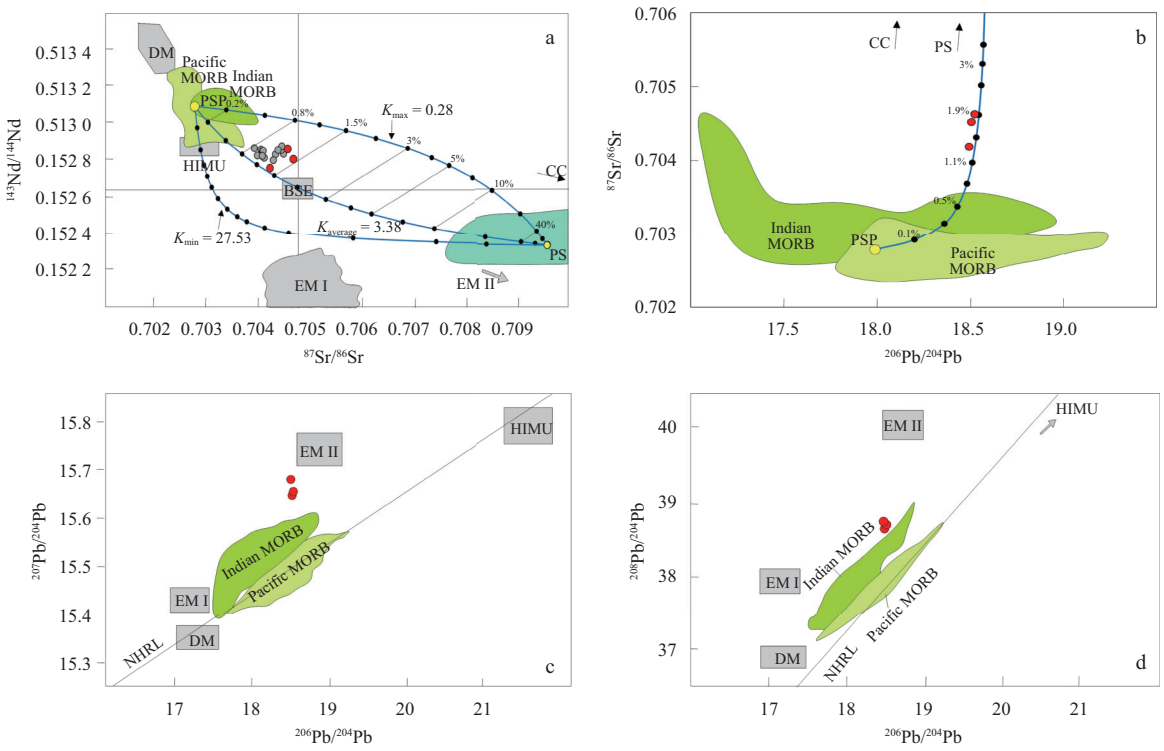

Fig. 6. Plots of the Sr, Nd and Pb isotope data in the IR rocks. The Pacific and Indian MORB data are based on Hofmann (1997) and Hickey-Vargas et al. (1995); CC is from Allègre et al. (1987); NHRL is from Hart (1984). The isotopic compositions of the IR rocks can be reasonably explained by the mixing of a Philippine Sea MORB-type source (PSP) and pelagic sediment (PS). a. $^{143}Nd/^{144}Nd$ versus $^{87}Sr/^{86}Sr$ diagram. The mixing ratio of PSP and PS was calculated using simulations. PSP representing the Indian MORB and its trace element concentrations are from Salters and Stracke (2004); isotopic compositions are represented by Shikoku and Parece Vela Basin rocks (Hickey-Vargas, 1991, 1998). Trace element and isotopic compositions of the PS area (average composition: $^{87}Sr/^{86}Sr$=0.709 54, $^{143}Nd/^{144}Nd$=0.512 34, Sr=1.89×10^{-4}, Nd=4.6×10^{-5}) are adopted from ODP Site 1149A, as published by Hauff et al. (2003). (K=(Nd/Sr)$_{PS}$/(Nd/Sr)$_{PSP}$, and K_{max} and K_{min} represent maximum and minimum values, respectively. $K_{average}$ represents the ratio of the average Sr and Nd concentrations of PS and PSP). The thin line connecting the two mixing lines is used to confirm and limit the mixing ratio between PS and PSP. b. $^{87}Sr/^{86}Sr$ versus $^{206}Pb/^{204}Pb$ diagram. Trace element and isotopic compositions of PSP and PS are also from Salters and Stracke (2004), Hickey-Vargas(1991, 1998) and Hauff et al. (2003). The average composition of PS is $^{87}Sr/^{86}Sr$=0.709 54, $^{206}Pb/^{204}Pb$=18.61, Sr=1.89×10^{-4}, Pb=1.8×10^{-5} (Hauff et al., 2003). c. $^{208}Pb/^{204}Pb$ versus $^{206}Pb/^{204}Pb$ diagram. d. $^{207}Pb/^{204}Pb$ versus $^{206}Pb/^{204}Pb$ diagram. The symbols are consistent with those in Fig. 4.

shown in Figs 7a and b, with increasing SiO_2, the ratios of $^{87}Sr/^{86}Sr$ and $^{144}Nd/^{143}Nd$ remain nearly constant; as a result, this may indicate that continental crust materials were not injected into the magma source of the IR rocks.

Figures 6c and d show that Pb isotopic ratios point to EMII, which indicates that an enriched component exists in the mantle source. Furthermore, the IR rocks record the signatures of the enrichment of the LILE compared with the HFSE and the REE, as well as positive Pb anomalies and negative Ti anomalies; these can be reasonably explained by the derivation of these rocks from an enriched mantle source containing a large amount of subduction components (Yang et al., 2017). Owing to the presence of low

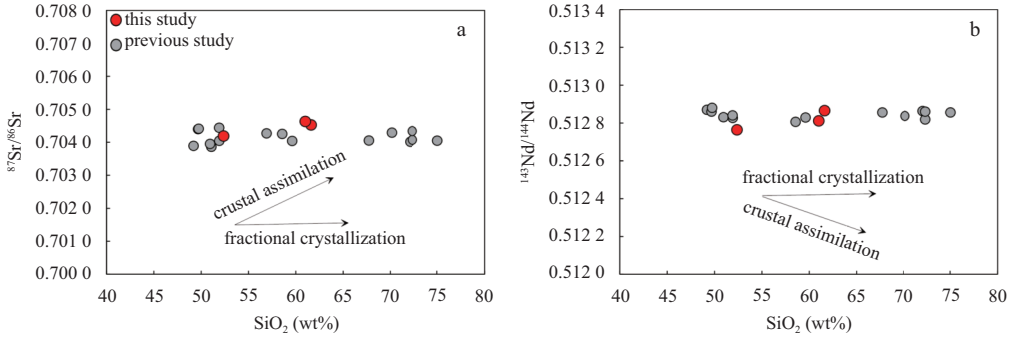

Fig. 7. SiO_2 versus $^{87}Sr/^{86}Sr$ plots (a) and SiO_2 versus $^{143}Nd/^{144}Nd$ plots (b). These plots indicate that crustal assimilation has a minor influence on the magmatic evolution of the IR rocks.

concentrations of Nb and Ta and high concentrations of Pb in subduction sediments (Plank and Langmuir, 1998), the generated rocks would inherit these characteristics if the subducted sediment components were indeed enriched in the mantle source (Niu et al., 2012). In addition, in our study, the Nd/Pb ratios (1.6–6.1) of the IR rocks are much lower than that of the general depleted MORB mantle (≈24; Class et al., 2000; Miller et al, 1994; Hofmann et al., 1986; Park et al., 2010), which suggests that a large quantity of a Pb-rich component, such as subducted sediment, is present in the magma source, because the Pb content of sediments is two orders of magnitude higher than that of the mantle (Yang et al., 2017). Thus, the addition of a small amount of sediments to the mantle source could cause a large reduction in its resulting Nd/Pb ratio.

Incompatible elements, due to their similar partition coefficients in magma, are rarely modified by the processes of partial melting or crystallization during magmatic activity (Duan et al., 2014); therefore, the ratios of incompatible elements can be used to determine the composition of the mantle source. Ba/La ratios are good indicators of the presence of subduction components (Taylor and Martinez, 2003). Ce/Pb ratios are comparatively stable in sediment, where they are much lower than they are in the mantle. Furthermore, Ce/Pb ratios do not obviously change during partial melting, fractional crystallization or other magma evolution processes (White and Duncan, 1996). Therefore, we used the ratios of Ba/La and Ce/Pb to determine the different magma sources of these rocks. Figure 8b shows that on the Ba/La versus Ce/Pb diagram, the IR rocks fall in the subducted sediments field, thus implying that subduction sediments largely contributed to the magma source. Simultaneously, the presence of lower Ce/Pb ratios in the IR rocks than in E-MORB and N-MORB also supports the presence of a Pb-rich component in the magma source.

The LILEs, such as Cs Rb, Ba, K, Sr, and Pb, mainly migrate in fluid phases, whereas the HFSEs (Th, U, Ce, Zr, Hf, Ti, Nb, Ta) mainly migrate in the melt phase (Elliott et al., 1997; Pearce and Peate, 1995; Class et al., 2000). Therefore, if rocks have high Ba/Th ratios, they may have been affected by aqueous fluid that was derived from the slab (Elliott et al., 1997; Pearce and Peate, 1995), whereas high Th/Nb ratios can represent slab-derived melts (Class et al., 2000; Johnson and Plank, 2000). In our study, the IR rocks record relatively high Th/Nb ratios (0.17–1.18) and low Ba/Th ratios (53.20–124.14) (Fig. 8a), which may suggest that compared to slab-derived fluid, sediment-derived melt is the main subduction component that was involved in the IR magma source (Luo et al., 2012).

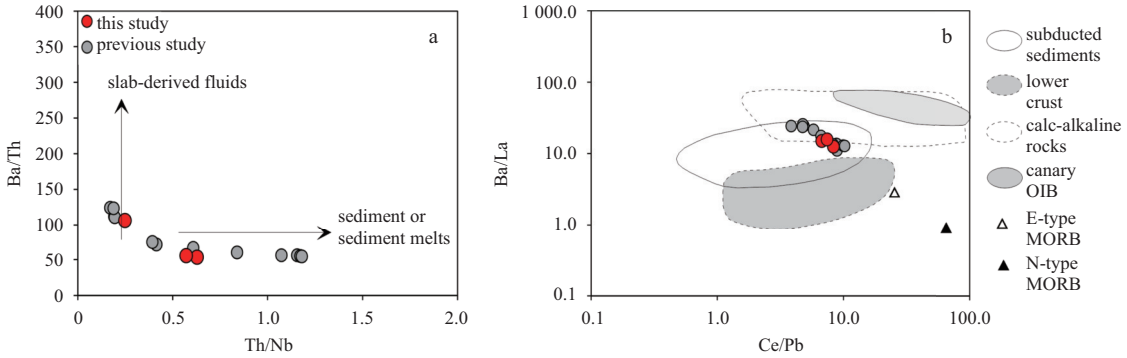

Fig. 8. Ba/Th versus Th/Nb diagram (a; Elliott et al., 1997) and Ba/La versus Ce/Pb trace element ratios in the IR volcanic rocks (b). Representative components of subducted sediments (Plank and Langmuir, 1998), lower crust (as represented by the North China Craton) (Liu et al., 2010), calc-alkaline basalt (Zhang and Sun, 2002; Zhang et al., 2009), Canary Island ocean island basalt (OIB; Prægel and Holm, 2006), and E-MORB and N-MORB (Sun and McDonough, 1989) are also shown.

5.3 *Petrogenesis of the IR rocks*

5.3.1 *Crystallization of minerals from the primitive melt*

As mentioned above, all of these rock suites record evidence of insignificant crustal contamination; thus, very little AFC may occur during magma evolution. Furthermore, the evolved characteristics of these rocks, along with their low $Mg^{\#}$ (<0.63) and continuous changes in major element compositions, further indicate that fractional crystallization may be the primary mechanism of magma evolution in this system (Guo et al., 2014).

Major oxides versus SiO_2 variation diagrams (Fig. 9) record continuously changing trends that closely resemble the typical evolution of fractional crystallization, in which olivine, clinopyroxene, and plagioclase are the main crystallizing minerals (Park et al., 2010).

The fact that Ni decreases with decreasing MgO may indicate that olivine fractionally crystallized from this magma (Fig. 10a). The negative correlation observed between SiO_2 and CaO shows that CaO-rich phases, such as amphibole, plagioclase or pyroxene, may have been involved during crystallization (Fig. 9) (Zhang et al., 2010). The positive correlation observed between Sr and Al_2O_3 (Fig. 11a) may reflect the removal of plagioclase (Cai et al., 2014). The slight positive Eu anomalies observed in basic rocks but more obvious negative Eu anomalies observed in intermediate to acid rocks (Figs 5f, d and b) indicate that plagioclase crystallization occurred during the transition from basic to acid magmas (Guo et al., 2016). When MgO content is less than 2 wt%, the Al_2O_3 content decreases rapidly, which suggests that this stage is mainly controlled by plagioclase crystallization (Fig. 11b) (Park et al., 2010). The CaO/Al_2O_3 ratios of the IR rocks show clear positive correlations with MgO and obvious negative correlations with Na_2O (Figs 11c and d), because the crystallization of clinopyroxene results in significant changes in the CaO/Al_2O_3 ratios (Zhang et al., 2010; Chun et al., 2015). Furthermore, accessory minerals are also involved in fractional crystallization during the process of magma evolution. When MgO conten is less than 4 wt%, the contents of TiO_2 and FeOt decrease synchronously with decreasing MgO (Figs 10b and d), which suggests that Fe-Ti ox-

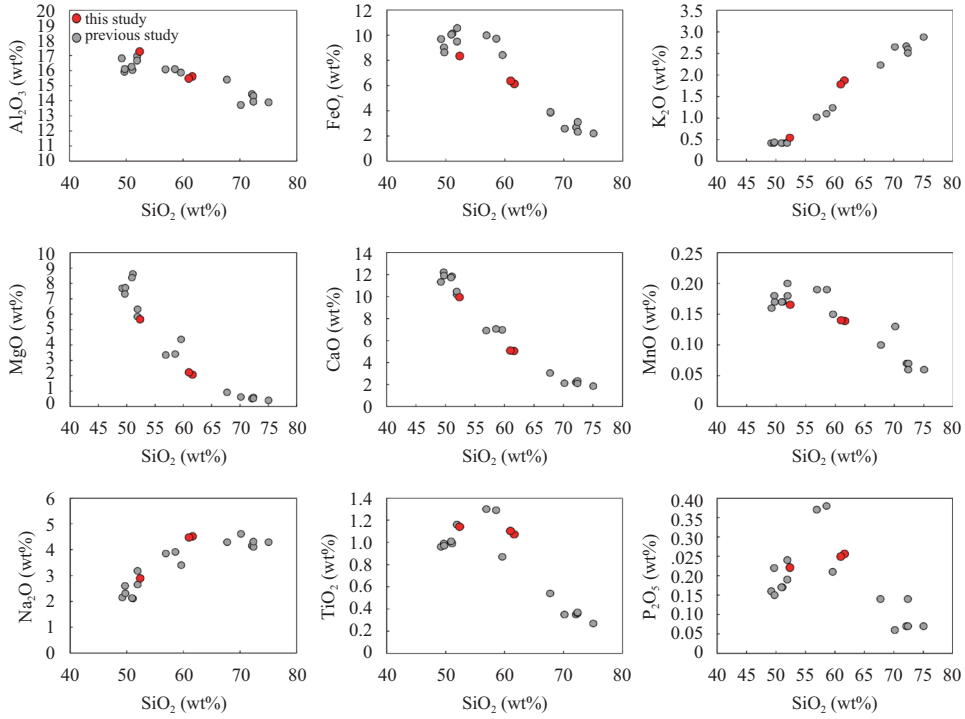

Fig. 9. Major oxides of basic to intermediate-acid rocks versus SiO_2 diagrams.

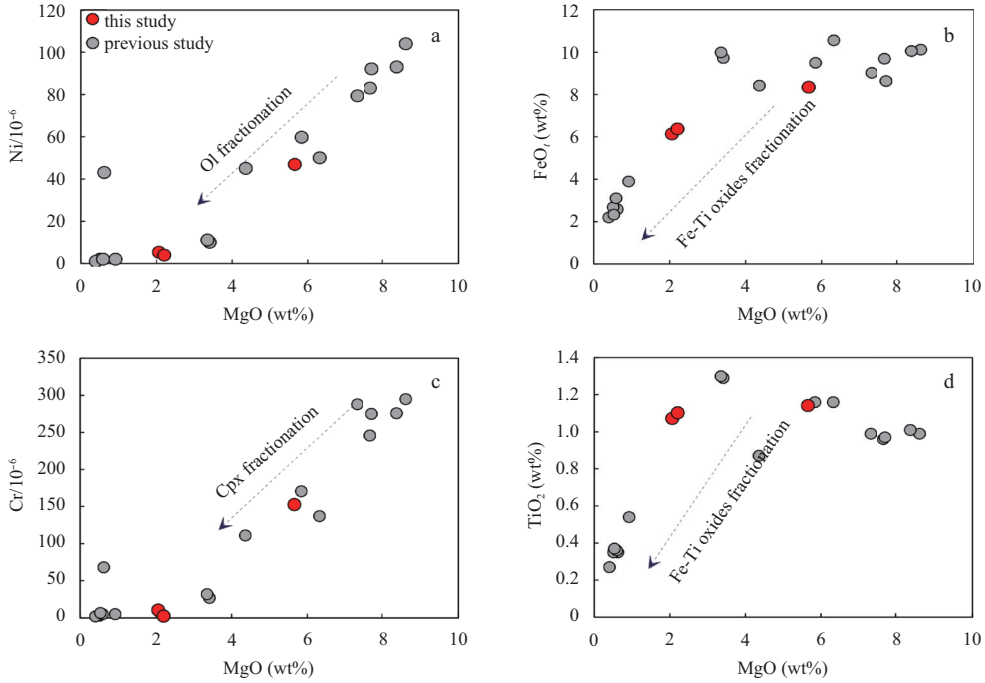

Fig. 10. MgO versus Ni, FeO_t, Cr and TiO_2. Arrows represent the fractional crystallization of olivine, clinopyroxene and Fe-Ti oxides with decreasing MgO content.

ides, such as magnetite and ilmenite, were fractionated from the magma (Guo et al., 2014; Zhang et al., 2016), which corresponds with petrographic observations (Fig. 3b). P_2O_5 sharply decreases when SiO_2 content is more than 57 wt% (Fig. 9), thus suggesting that apatite was also a fractionating mineral (Park et al., 2010).

5.3.2 *Origin of the intermediate-acid magma*

Figure 1 shows that all of these rock samples were collected within a small space, with a maximum distance between these different sites being less than 20 km. Moreover, these samples are distributed along the same elongated volcanic ridge that can be seen in Google Earth (Lai et al., 2016). It is worth noting that the typical first-order trends shown in the major element oxides versus SiO_2 diagrams (Fig. 9) imply an evolution process of the fractional crystallization of magma (Hu et al., 2016). Furthermore, the similar isotopic compositions of the basic and interme-

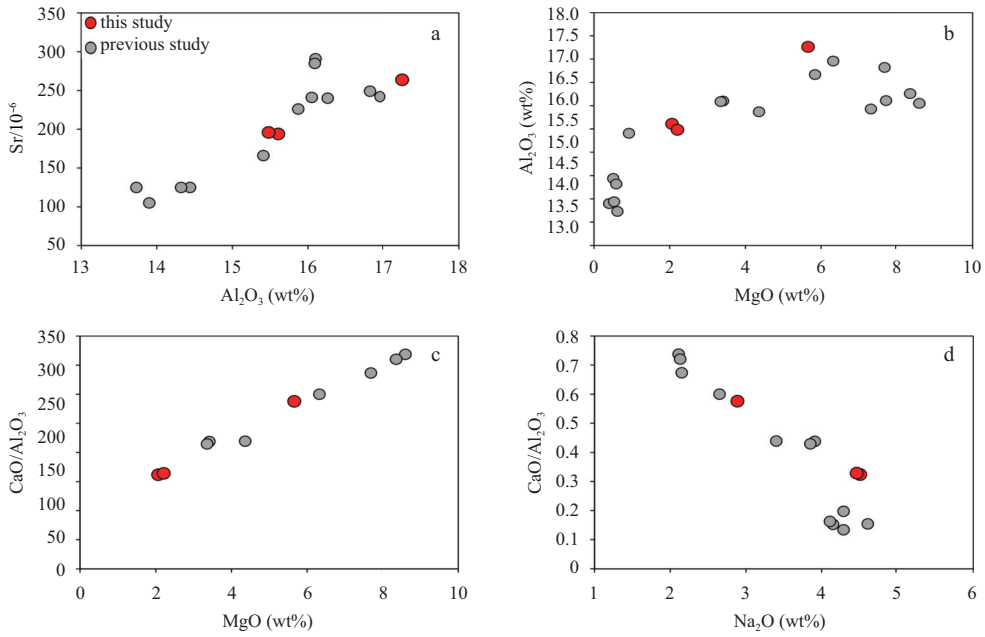

Fig. 11. Al_2O_3 versus Sr and MgO (a, b) and CaO/Al_2O_3 versus MgO (c) and Na_2O (d). The correlational relationships in these diagrams could be produced via fractional crystallization.

diate-acid rocks may demonstrate that they share a genetic link through fractional crystallization (Hu et al., 2016) (Fig. 6).

There are two major genetic mechanisms that can generate intermediate-acid magmas when producing volcanic rocks with bimodal characteristics (Wang et al., 2006, 2010). One is the partial melting of continental crustal material with a basaltic magma heat source (Christiansen, 1984); these melts record the characteristics of negative $\varepsilon Nd(t)$ values, distinct trace element compositions and variable Sr-Nd-Pb isotopic compositions (Doe et al., 1982; Davies and MacDonald, 1987). The second cause is the fractional crystallization of basaltic magma with little to no continental crust material contamination (Bacon and Druitt, 1988; MacDonald et al., 1987; Grove and Donnelly-Nolan, 1986); these melts have the same trace element distribution patterns and Sr-

Table 4. Values of partition coefficients (d) used in modeling

Elements	Ol[1)]	Cpx[1)]	Cpx[2)]	Pl[1)]	Pl[2)]	Amph[2)]	Mt[1)]	Mt[2)]	Ap[2)]	Bulk D[1)]	Bulk D[2)]
Rb	0.009 8	0.031	0.032	0.071	0.041	0.400	0.01	0.010	0.40	0.049	0.074
Ba	0.009 9	0.026	0.131	0.230	0.308	0.300	0.01	0.100	0.45	0.135	0.271
Nb	0.010 0	0.005	0.800	0.010	0.060	4.000	0.40	2.500	0.10	0.048	0.668
Ta	0.030 0	0.013	0.263	0.027	0.035	0.430	1.00	2.000	0.05	0.121	0.205
K	0.006 8	0.038	0.037	0.170	0.100	0.081	0.01	0.045	–	0.105	0.085
La	0.006 7	0.056	0.015	0.190	0.380	0.360	1.50	0.300	14.50	0.269	0.390
Ce	0.006 0	0.092	0.044	0.120	0.267	0.680	1.30	0.300	21.10	0.220	0.379
Sr	0.014 0	0.060	0.516	1.830	1.600	0.010	0.01	0.077	1.30	1.024	1.209
Nd	0.005 9	0.310	0.166	0.081	0.203	1.600	1.00	0.300	32.80	0.223	0.498
Sm	0.007 0	0.500	0.457	0.067	0.165	2.300	1.10	0.300	46.00	0.273	0.648
Zr	0.012 0	0.100	0.600	0.048	0.135	0.500	0.10	0.800	0.10	0.063	0.273
Hf	0.013 0	0.263	0.633	0.051	0.150	0.520	2.00	1.000	0.73	0.295	0.303
Eu	0.006 8	0.510	0.411	0.376	0.443	3.200	0.60	0.300	30.40	0.395	0.843
Ti	0.020 0	0.400	0.700	0.040	0.050	7.000	7.50	12.500	0.10	0.874	1.431
Gd	0.007 7	0.610	0.703	0.063	0.125	5.480	0.300	0.300	43.90	0.218	0.948
Dy	0.009 6	0.680	0.776	0.055	0.112	6.200	1.00	0.370	50.70	0.301	1.056
Y	0.010 0	0.900	0.900	0.030	0.130	6.000	0.20	2.000	40.00	0.263	1.002
Er	0.011 0	0.650	1.800	0.063	0.084	5.940	1.00	0.300	37.20	0.298	1.094
Yb	0.014 0	0.620	1.580	0.067	0.090	4.890	1.00	0.550	23.90	0.293	0.912
Lu	0.016 0	0.560	1.540	0.060	0.092	4.530	1.00	0.740	20.20	0.275	0.864

Note: The values of distribution coefficients are from Arth (1976), Fujimaki et al. (1984), Pearce and Norry (1979), Schock (1979), Gill (1981), Philpotts and Schnetzler (1970), Nash and Crecraft (1985), Mahood and Hildreth (1983), Fujimaki (1986), Shinjo and Kato (2000), Lemarchand et al. (1987), Dunn and Sen (1994), Bacon and Druitt (1988), Ewart and Griffin (1994), Sisson (1991), and Mahood and Stimac (1990). The formula of $C_L/C_0=F^{(D-1)}$ is used as the fractional crystallization model. C_L is the trace element weight concentration in the residual liquid; C_0 is the trace element weight concentration in the parental liquid; Bulk D is the bulk distribution coefficient of the fractionating assemblage and F is the fraction of the remaining melt. [1)] and [2)] represent the basaltic-andesitic and rhyolitic liquids, respectively; and – not collected.

Nd isotopic ratios as basaltic magma (Brouxel et al., 1987; Geist et al., 1995). The intermediate-acid rock samples and basic rock samples from the IR have similar trace element distributions, which are manifested by the enrichment of the LILE compared with HFSE and the REE and the depletions of Nb, Ta, and Ti (Fig. 5). In addition, all of these rock samples yield comparatively uniform Sr-Nd isotopic ratios (Fig. 6) and εNd(0) values that are greater than 0 (+2.44 to +4.72). The trace element and Sr-Nd isotopic characteristics of these samples indicate that this intermediate-acid magma was generated by the fractional crystallization of basaltic magma. The presence of accessory phases can also profoundly influence the trace element characteristics of hydrous melts, because these phases control several trace elements (Ti^{4+} can replace Fe^{3+}, which can then enter magnetite; P is consumed to produce apatite) (Hermann and Rubatto, 2009). In addition, the elements of Sr and Eu can both enter plagioclase in the early stages of fractional crystallization of magma, which can deplete the evolved magma in those elements (Guo, 2016). In the IR rocks, basic rocks record positive anomalies of P, Sr, and Eu and slightly negative Ti concentration anomalies, while the intermediate-acid rocks record strong negative anomalies of those elements (Fig. 5), which also demonstrate that the generation of intermediate-acid magma may be the result of the fractional crystallization of basic magma.

We also carried out simulated calculations of fractional crystallization by increasing the fractionation level to determine the effect of fractional crystallization on the trace element compositions of the original melt (Table 4, Fig. 12). We used the average composition of basaltic rocks to represent the initial magma composition or the composition of the magma during an early stage of its evolution. The types and proportions of minerals estimated using this process are in reasonable agreement with petrographic observations. In intermediate rocks, approximately 10% olivine, 25% clinopyroxene, 55% plagioclase and 10% magnetite were crystallized; in acid rocks, approximately 15% clinopyroxene, 70% plagioclase, 9.5% amphibole, 5.0% magnetite and 0.5% apatite were crystallized. As a result, these simulations suggest that approximately 60% fractionation of an initial basaltic magma can produce the trace element compositions that are similar to those of intermediate rocks (Fig. 12a), and 75% fractional crystallization of a basaltic magma can produce compositions that are similar to those of acid rocks (Fig. 12b). Therefore, we conclude that in the IR, different degrees of fractional crystallization of the corresponding basaltic magma, crystallizing olivine, clinopyroxene, plagioclase, amphibole, magnetite and apatite, can generate the observed compositions of the intermediate and acid rocks.

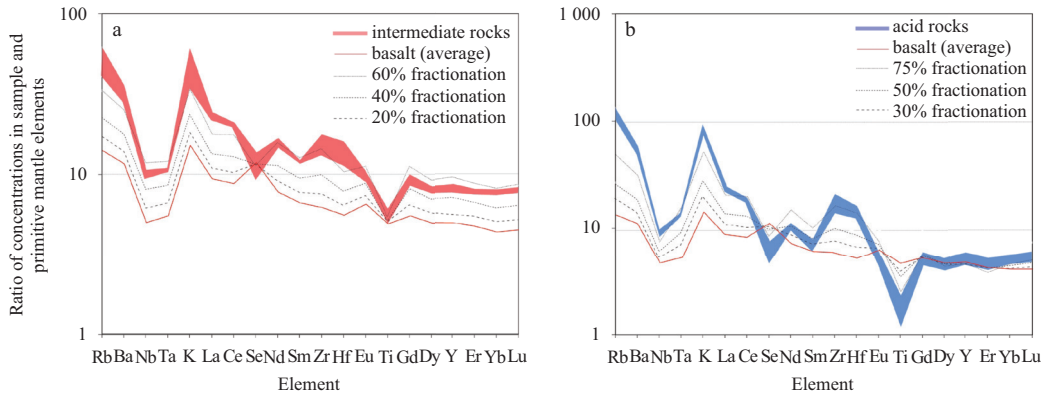

Fig. 12. Simulated calculations of trace element compositions produced by fractional crystallization of primitive melt. a. Different degrees of fractionation (20%, 40% and 60%) of basaltic magma to produce intermediate rocks. Proportions of the residual assemblage are 0.10 Ol+0.25 Cpx+0.55 Pl+0.10 Mt. b. Different degrees of fractionation (30%, 50% and 75%) of basaltic magma to produce acid rocks. Proportions of the residual assemblage are 0.15 Cpx+0.70 Pl+0.095 Amph+0.05 Mt+0.005 Ap. Ol represents Olivine, Cpx clinopyroxene, Pl plagioclase, Amph Amphibole, Mt Magnetite, and Ap Apatite.

6 Conclusions

In this study, we present a study of the petrographic and geochemical compositions of the rock samples from the IR in the MOT with the following three points:

(1) The Iheya Ridge rocks studied here were derived from a similar magma source that underwent the fractional crystallization of olivine, clinopyroxene, plagioclase, and amphibole, as well as accessory minerals, which may have been the main mechanism of magma evolution;

(2) The intermediate rocks and acid rocks erupted from the Iheya Ridge could have originated from approximately 60% and 75% fractionation, respectively, of an evolved homologous basaltic magma;

(3) Subducted sediment was probably involved in the mantle magma source of the Iheya Ridge volcanic rocks, which may have comprised a mixture of 0.8%–2.0% subduction sediment components and 98.0%–99.2% mantle-derived melts.

Acknowledgements

The authors extend their heartfelt thanks to the Institute of Oceanology, Chinese Academy of Sciences for the supplied samples, Liu Hongyan for help with the analysis of major elements, and Yin Xuebo for help with the analysis of the trace elements of samples.

References

Allègre C J, Hamelin B, Provost A, et al. 1987. Topology in isotopic multispace and origin of mantle chemical heterogeneities. Earth and Planetary Science Letters, 81(4): 319–337

Arth J G. 1976. Behaviour of trace elements during magmatic processes—A summary of theoretical models and their applications. Journal of Research of the U.S. Geological Survey, 4(1): 41–47

Bacon C R, Druitt T H. 1988. Compositional evolution of the zoned calcalkaline magma chamber of Mount Mazama, Crater Lake, Oregon. Contributions to Mineralogy and Petrology, 98(2):

224–256
Brouxel M, Lapierre H, Michard A, et al. 1987. The deep layers of a Paleozoic arc: geochemistry of the Copley-Balaklala series, northern California. Earth and Planetary Science Letters, 85(4): 386–400
Cai Yachun, Fan Hongrui, Santosh M, et al. 2014. Silicate melt inclusions in clinopyroxene phenocrysts from mafic dikes in the eastern North china Craton: constraints on melt evolution. Journal of Asian Earth Sciences, 97: 150–168
Christiansen R L. 1984. Yellowstone magmatic evolution: its bearing on understanding large-volume explosive volcanism. In: Explosive Volcanism: Inception, Evolution, and Hazards. Washington, DC: National Academy Press, 84–95
Chun Minghao, Yu Zenghui, Zhai Shikui. 2015. The geochemistry and geological significances of basalts from Carlsberg Ridge in Indian Ocean. Haiyang Xuebao (in Chinese), 37(8): 47–62
Class C, Miller D M, Goldstein S L, et al. 2000. Distinguishing melt and fluid subduction components in Umnak volcanics, Aleutian arc. Geochemistry, Geophysics, Geosystems, 1(6): 1004
Davies G R, MacDonald R. 1987. Crustal influences in the petrogenesis of the Naivasha basalt-comendite complex: combined trace element and Sr-Nd-Pb isotope constraints. Journal of Petrology, 28(6): 1009–1031
Doe B R, Leeman W P, Christiansen R L, et al. 1982. Lead and strontium isotopes and related trace elements as genetic tracers in the Upper Cenozoic rhyolite-basalt association of the Yellowstone Plateau Volcanic Field. Journal of Geophysical Research: Atmospheres, 87(B6): 4785–4806
Duan Xianzhe, Sun He, Yang Wei, et al. 2014. Melt-peridotite interaction in the shallow lithospheric mantle of the North China Craton: evidence from melt inclusions in the quartz-bearing orthopyroxene-rich websterite from Hannuoba. International Geology Review, 56(4): 448–472
Dunn T, Sen C. 1994. Mineral/matrix partition-coefficients for orthopyroxene, plagioclase, and olivine in basaltic to andesitic systems: a combined analytical and experimental study. Geochimica et Cosmochimica Acta, 58(2): 717–733, doi: 10.1016/0016–7037(94)90501–0
Elliott T, Plank T, Zindler A, et al. 1997. Element transport from slab to volcanic front at the Mariana arc. Journal of Geophysical Research: Atmospheres, 102(B7): 14991–15019
Ewart A, Griffin W L. 1994. Application of proton-microprobe data to trace-element partitioning in volcanic-rocks. Chemical Geology, 117(1–4), 251–284, doi: 10.1016/0009–2541(94)90131–7
Fujimaki H. 1986. Partition coefficients of Hf, Zr, and REE between zircon, apatite, and liquid. Contributions to Mineralogy and Petrology, 94(1): 42–45
Fujimaki H, Tatsumoto M, Aoki K I. 1984. Partition coefficients of Hf, Zr, and ree between phenocrysts and groundmasses. Journal of Geophysical Research: Atmospheres, 89(S02): B662–B672
Gao Jinyao, Zhang Tao, Fang Yinxia, et al. 2009. Faulting, magmatism and crustal oceanization of the Okinawa Trough. Acta Oceanologica Sinica, 28(3): 40–49
Geist D, Howard K A, Larson P. 1995. The generation of oceanic rhyolites by crystal fractionation: the basalt-rhyolite association at Volcán Alcedo, Galápagos Archipelago. Journal of Petrology, 36(4): 965–982
Gill J B. 1981. Orogenic Andesites and Plate Tectonics. New York: Springer
Grove T L, Donnelly-Nolan J M. 1986. The evolution of young silicic lavas at Medicine Lake volcano, California: implications for the origin of compositional gaps in calc-alkaline series lavas. Contributions to Mineralogy and Petrology, 92(3): 281–302
Guo Kun. 2016. Volcanic rock magma source composition and subduction composition effects in Okinawa Trough (in Chinese) [dissertation]. Qingdao: Ocean University of China
Guo Pengyuan, Niu Yaoling, Sun Pu, et al. 2016. The origin of Cenozoic basalts from central Inner Mongolia, East China: the consequence of recent mantle metasomatism genetically associated with seismically observed paleo-Pacific slab in the mantle transition zone. Lithos, 240–243: 104–118
Guo Pengyuan, Niu Yaoling, Ye Lei, et al. 2014. Lithosphere thinning beneath west North China craton: evidence from geochemical and Sr-Nd-Hf isotope compositions of Jining basalts. Lithos, 202–203: 37–54
Hart S R. 1984. A large-scale isotope anomaly in the Southern Hemisphere mantle. Nature, 309(5971): 753–757
Hauff F, Hoernle K, Schmidt A. 2003. Sr-Nd-Pb composition of Mesozoic Pacific oceanic crust (Site 1149 and 801, ODP Leg 185): implications for alteration of ocean crust and the input into the Izu-Bonin-Mariana subduction system. Geochemistry, Geophysics, Geosystems, 4(8): 8913, doi: 10.1029/2002GC000421
Hermann J, Rubatto D. 2009. Accessory phase control on the trace element signature of sediment melts in subduction zones. Chemical Geology, 265(3–4): 512–526
Hickey-Vargas R. 1991. Isotope characteristics of submarine lavas from the Philippine Sea: implications for the origin of arc and basin magmas of the Philippine tectonic plate. Earth and Planetary Science Letters, 107(2): 290–304
Hickey-Vargas R. 1998. Origin of the Indian Ocean-type isotopic signature in basalts from Philippine Sea plate spreading centers: an assessment of local versus large-scale processes. Journal of Geophysical Research: Atmospheres, 103(B9): 20963–20979
Hickey-Vargas R, Hergt J M, Spadea P. 1995. The Indian Ocean-type isotopic signature in western Pacific marginal basins: origin and significance. In: Taylor B, Natland J, eds. Active Margins and Marginal Basins of the Western Pacific. Active Margins and Marginal Basins of the Western Pacific, 175–197
Hoang N, Uto K. 2006. Upper mantle isotopic components beneath the Ryukyu arc system: evidence for 'back-arc' entrapment of Pacific MORB mantle. Earth and Planetary Science Letters, 249(3–4): 229–240
Hofmann A W. 1997. Mantle geochemistry: the message from oceanic volcanism. Nature, 385(6613): 219–229
Hofmann A W, Jochum K P, Seufert M, et al. 1986. Nb and Pb in oceanic basalts: new constraints on mantle evolution. Earth and Planetary Science Letters, 79(1–2): 33–45
Honma H, Kusakabe M, Kagami H, et al. 1991. Major and trace element chemistry and D/H, $^{18}O/^{16}O$, $^{87}Sr/^{86}Sr$ and $^{143}Nd/^{144}Nd$ ratios of rocks from the spreading center of the Okinawa Trough, a marginal back-arc basin. Geochemical Journal, 25(2): 121–136
Hu Yan, Niu Yaoling, Li Jiyong, et al. 2016. Petrogenesis and tectonic significance of the Late Triassic mafic dikes and felsic volcanic rocks in the East Kunlun Orogenic Belt, Northern Tibet Plateau. Lithos, 245: 205–222
Huang Peng, Li Anchun, Jiang Hengyi. 2006. Geochemical features and their geological implications of volcanic rocks from the northern and middle Okinawa Trough. Acta Petrologica Sinica (in Chinese), 22(6): 1703–1712
Irvine T N, Baragar W R A. 1971. A guide to the chemical classification of the common volcanic rocks. Canadian Journal of Earth Sciences, 8(5): 523–548
Ishikawa M, Sato H, Furukawa M, et al. 1991. Report on DELP 1988 cruises in the Okinawa Trough: part 6. Petrology of volcanic rocks. Bulletin of the Earthquake Research Institute, University of Tokyo, 66(1): 151–177
Ishizuka H, Kawanobe Y, Sakai H. 1990. Petrology and geochemistry of volcanic rocks dredged from the Okinawa Trough, an active back-arc basin. Geochemical Journal, 24(2): 75–92
Ishizuka O, Taylor R N, Yuasa M, et al. 2007. Processes controlling along-arc isotopic variation of the southern Izu-Bonin arc. Geochemistry, Geophysics, Geosystems, 8(6): Q06008
Johnson M C, Plank T. 2000. Dehydration and melting experiments constrain the fate of subducted sediments. Geochemistry, Geophysics, Geosystems, 1(12): 1007
Kimura M. 1985. Back-arc rifting in the Okinawa Trough. Marine and Petroleum Geology, 2(3): 222–240
Kimura M, Kaneoka I, Kato Y, et al. 1986. Report on DELP 1984 cruises in the middle Okinawa Trough: Part 5. Topography and geology of the central grabens and their vicinity. Bulletin of the Earthquake Research Institute, University of Tokyo, 61(2):

269–310
Kimura M, Kato Y, Tanaka T, et al. 1987. Submersible SHINKAI 2000 study on the central rift in the middle Okinawa Trough. In: 3rd Symposium on Deep-Sea Research Using the Submersible "SHINKAI 2000" System. Yokosuka: Japan Marine Science and Technology Center, 165–196
Kimura M, Oomori T, Izawa E, et al. 1991. Research results of the 284, 286, 287 and 366 dives in the Iheya Depression and the 364 dive in the Izena Holl by "SHINKAI 2000". In: 7th Symposium on Deep-sea Research Using the Submersible "Shinkai 2000" System. Yokosuka: Japan Marine Science and Technology Center, 147–161
Lai Zhiqing, Zhao Guangtao, Han Zongzhu, et al. 2016. Back-arc magma processes in the Okinawa Trough: new insights from textural and compositional variations of plagioclase in basalts. Geological Journal, 51(S1): 346–356
Lee C S, Shor Jr G G, Bibee L D, et al. 1980. Okinawa Trough: origin of a back-arc basin. Marine Geology, 35(1–3): 219–241
Lemarchand F, Villemant B, Calas G. 1987. Trace element distribution coefficients in alkaline series. Geochimica et Cosmochimica Acta, 51(5): 1071–1081, doi: 10.1016/0016–7037(87)90201–8
Letouzey J, Kimura M. 1985. Okinawa Trough genesis: structure and evolution of a backarc basin developed in a continent. Marine and Petroleum Geology, 2(2): 111–130
Letouzey J, Kimura M. 1986. The Okinawa Trough: genesis of a back-arc basin developing along a continental margin. Tectonophysics, 125(1–3): 209–230
Li Naisheng. 2001. On tectonic problems of the Okinawa Trough. Chinese Journal of Oceanology and Limnology, 19(3): 255–264
Li Weiran, Yang Zuosheng, Wang Yongji, et al. 1997. The petrochemical features of the volcanic rocks in Okinawa Trough and their geological significance. Acta Petrologica Sinica (in Chinese), 13(4): 538–550
Liu Yongsheng, Gao Shan, Gao Changgui, et al. 2010. Garnet-rich granulite xenoliths from the Hannuoba basalts, North China: petrogenesis and implications for the Mesozoic crust-mantle interaction. Journal of Earth Science, 21(5): 669–691
Luo Biji, Zhang Hongfei, Lü Xinbiao. 2012. U-Pb zircon dating, geochemical and Sr-Nd-Hf isotopic compositions of Early Indosinian intrusive rocks in West Qinling, central China: petrogenesis and tectonic implications. Contributions to Mineralogy and Petrology, 164(4): 551–569
MacDonald R, Davies G R, Bliss C M, et al. 1987. Geochemistry of high-silica peralkaline rhyolites, Naivasha, Kenya rift valley. Journal of Petrology, 28(6): 979–1008
Mahood G, Hildreth W. 1983. Large partition coefficients for trace elements in high-silica rhyolites. Geochimica et Cosmochimica Acta, 47(1): 11–30
Mahood G A, Stimac J A. 1990. Trace-element partitioning in pantellerites and trachytes. Geochimica et Cosmochimica Acta, 54(8): 2257–2276, doi: 10.1016/0016–7037(90)90050-U
Maitre R W L. 1989. A Classification of Igneous Rocks and Glossary of Terms. Oxford: Blackwell
Miki M, Matsuda T, Otofuji Y. 1990. Opening mode of the Okinawa Trough: paleomagnetic evidence from the South Ryukyu Arc. Tectonophysics, 175(4): 335–347
Miller D M, Goldstein S L, Langmuir C H. 1994. Cerium/lead and lead isotope ratios in arc magmas and the enrichment of lead in the continents. Nature, 368(368): 514–520
Nash W P, Crecraft H R. 1985. Partition coefficients for trace elements in silicic magmas. Geochimica et Cosmochimica Acta, 49(11): 2309–2322
Niu Y L, Wilson M, Humphreys E R, et al. 2012. A trace element perspective on the source of ocean island basalts (OIB) and fate of subducted ocean crust (SOC) and mantle lithosphere (SML). Episodes, 35(2): 310–327
Okino K, Tokuyama H, HOTWATER Scientific Party. 2002. Deep-tow sonar "WADATSUMI" survey in the Okinawa Trough. InterRidge News, 11(2): 36–39
Park S H, Lee S M, Kamenov G D, et al. 2010. Tracing the origin of subduction components beneath the South East rift in the Manus Basin, Papua New Guinea. Chemical Geology, 269(3–4): 339–349
Pearce J A, Norry M J. 1979. Petrogenetic implications of Ti, Zr, Y, and Nb variations in volcanic rocks. Contributions to Mineralogy and Petrology, 69(1): 33–47
Pearce J A, Peate D W. 1995. Tectonic implications of the composition of volcanic arc magmas. Annual Review of Earth and Planetary Sciences, 23(1): 251–285
Philpotts J A, Schnetzler C C. 1970. Phenocryst-matrix partition coefficients for K, Rb, Sr and Ba, with applications to anorthosite and basalt genesis. Geochimica et Cosmochimica Acta, 34(3): 307–322
Plank T. 2005. Constraints from thorium/lanthanum on sediment recycling at subduction zones and the evolution of the continents. Journal of Petrology, 46(5): 921–944
Plank T, Langmuir C H. 1998. The chemical composition of subducting sediment and its consequences for the crust and mantle. Chemical Geology, 145(3–4): 325–394
Prægel N O, Holm P M. 2006. Lithospheric contributions to high-MgO basanites from the Cumbre Vieja volcano, La Palma, Canary Islands and evidence for temporal variation in plume influence. Journal of Volcanology and Geothermal Research, 149(3–4): 213–239
Rudnick R L, Gao S. 2003. Composition of the continental crust. In: Holland H D, Turekian K K, eds. Treatise on Geochemistry. 2nd ed. Amsterdam: Elsevier, 1–64
Salters V J M, Stracke A. 2004. Composition of the depleted mantle. Geochemistry, Geophysics, Geosystems, 5(5): Q05B07
Savov I P, Hickey-Vargas R, D'Antonio M, et al. 2006. Petrology and geochemistry of west Philippine basin basalts and early Palau-Kyushu arc volcanic clasts from ODP leg 195, site 1201D: implications for the early history of the Izu-Bonin-Mariana arc. Journal of Petrology, 47(2): 277–299
Schock H H. 1979. Distribution of rare-earth and other trace elements in magnetites. Chemical Geology, 26(1–2): 119–133
Shinjo R. 1999. Geochemistry of high Mg andesites and the tectonic evolution of the Okinawa Trough-Ryukyu arc system. Chemical Geology, 157(1–2): 69–88
Shinjo R, Chung S L, Kato Y, et al. 1999. Geochemical and Sr-Nd isotopic characteristics of volcanic rocks from the Okinawa Trough and Ryukyu arc: implications for the evolution of a young, intracontinental back arc basin. Journal of Geophysical Research: Solid Earth, 104(B5): 10591–10608
Shinjo R, Kato Y. 2000. Geochemical constraints on the origin of bimodal magmatism at the Okinawa Trough, an incipient back-arc basin. Lithos, 54(3–4): 117–137
Shinjo R, Woodhead J D, Hergt J M. 2000. Geochemical variation within the northern Ryukyu Arc: magma source compositions and geodynamic implications. Contributions to Mineralogy and Petrology, 140(3): 263–282
Sibuet J C, Letouzey J, Barbier F, et al. 1987. Back arc extension in the Okinawa Trough. Journal of Geophysical Research: Atmospheres, 92(B13): 14041–14063
Sisson T W. 1991. Pyroxene-high silica rhyolite trace-element partition coefficients measured by ion microprobe. Geochimica et Cosmochimica Acta, 55(6): 1575–1585, doi: 10.1016/0016-7037(91)90129-S
Sun S S, Mcdonough W F. 1989. Chemical and isotopic systematics of oceanic basalts; implications for mantle composition and processes. Geological Society, London, Special Publications, 42(1): 313–345
Taylor B, Martinez F. 2003. Back-arc basin basalt systematics. Earth and Planetary Science Letters, 210(3–4): 481–497
Wang K L, Chung S L, Chen C H, et al. 1999. Post-collisional magmatism around northern Taiwan and its relation with opening of the Okinawa Trough. Tectonophysics, 308(3): 363–376
Wang Yinxi, Gu Lianxing, Zhang Zunzhong, et al. 2006. Geochronology and Nd-Sr-Pb isotops of the bimodal volcanic rocks of the Bogda rift. Acta Petrologica Sinica (in Chinese), 22(5): 1215–1224
Wang Jinrong, Li Taide, Tian Liping, et al. 2010. Late Paleozoic tec-

tono-magmatic evolution in Bogda Orogenic Belt, Xinjiang: evidence from geochemistry of volcanic rocks. Acta Petrologica Sinica (in Chinese), 26(4): 1103–1115

Wang Shugong, Liang Ruicai, Wang Yong, et al. 1998. Gravity and magnetic characteristics of the north part of the Okinawa Trough and geological interpretation. Marine Geology & Quaternary Geology (in Chinese), 18(4): 19–27

White W M, Duncan R A. 1996. Geochemistry and geochronology of the Society Islands: new evidence for deep mantle recycling. In: Basu A, Hart S, eds. Earth Processes: Reading the Isotopic Code. Washington, DC: American Geophysical Union 95: 183–206

Yamano M, Uyeda S, Foucher J P, et al. 1989. Heat flow anomaly in the middle Okinawa Trough. Tectonophysics, 159(3–4): 307–318

Yan Quanshu, Shi Xuefa. 2014. Petrologic perspectives on tectonic evolution of a nascent basin (Okinawa Trough) behind Ryukyu arc: a review. Acta Oceanologica Sinica, 33(4): 1–12

Yang Shuying, Fang Nianqiao. 2015. Geochemical variation of volcanic rocks from the South China Sea and neighboring land: implication for magmatic process and mantle structure. Acta Oceanologica Sinica, 34(12): 112–124, doi: 10.1007/s13131–015-0759–8

Yang Yizeng, Wang Yan, Ye Risheng, et al. 2017. Petrology and geochemistry of Early Cretaceous A-type granitoids and late Mesozoic mafic dikes and their relationship to adakitic intrusions in the lower Yangtze River belt, Southeast China. International Geology Review, 59(1): 62–79

Zeng Zhigang, Yu Shaoxiong, Wang Xiaoyuan, et al. 2010. Geochemical and isotopic characteristics of volcanic rocks from the northern East China Sea shelf margin and the Okinawa Trough. Acta Oceanologica Sinica, 29(4): 48–61

Zhai Shikui, Chen Lirong, Wang Zhen, et al. 1997. Primary analysis on pumice magmatism model of the Okinawa Trough. Marine Geology & Quaternary Geology (in Chinese), 17(1): 59–66

Zhang Guoliang, Jiang Shaoqing, Ouyang Hegen, et al. 2010. Magma mixing in upper mantle: evidence from high $Mg^{\#}$ olivine hosted melt inclusions in MORBs near East Pacific Rise 13°N. Chinese Science Bulletin, 55(16): 1643–1656

Zhang Liangliang, Liu Chuanzhou, Wu Fuyuan, et al. 2016. Sr-Nd-Hf isotopes of the intrusive rocks in the Cretaceous Xigaze ophiolite, southern Tibet: constraints on its formation setting. Lithos, 258–259: 133–148

Zhang Hongfu, Sun Min. 2002. Geochemistry of Mesozoic basalts and mafic dikes, southeastern North China Craton, and tectonic implications. International Geology Review, 44(4): 370–382

Zhang Junjun, Zheng Yongfei, Zhao Zifu. 2009. Geochemical evidence for interaction between oceanic crust and lithospheric mantle in the origin of Cenozoic continental basalts in east-central China. Lithos, 110(1–4): 305–326

Correction instructions

Due to the negligence of the author, the foundation item “The NSFC-Shandong Joint Fund for Marine Science Research Centers under contract No. U150640007” in 2017, Vol. 36, No. 7, P. 77–85 is not correct, and should be changed to “The NSFC-Shandong Joint Fund for Marine Science Research Centers under contract No. U1606401”, hereby certify.